

Research Article

Exploring Cinnamic Acids as Potent Antimetastatic Agents for Cancer Therapy: Molecular Docking and Dynamic Simulation against MMP2

Setareh Shojaei ¹, Mohammad-Reza Zandieh ¹, Shokoofeh Jamshidi ¹, Amir Taherkhani ², and Zahra Azadian ²

¹Department of Oral and Maxillofacial Pathology, School of Dentistry, Hamadan University of Medical Sciences, Hamadan, Iran

²Research Center for Molecular Medicine, Hamadan University of Medical Sciences, Hamadan, Iran

Correspondence should be addressed to Amir Taherkhani; amir.007.taherkhani@gmail.com

Received 30 September 2023; Revised 1 January 2024; Accepted 26 March 2024; Published 17 April 2024

Academic Editor: Faisal Raza

Copyright © 2024 Setareh Shojaei et al. This is an open access article distributed under the Creative Commons Attribution License, which permits unrestricted use, distribution, and reproduction in any medium, provided the original work is properly cited.

Objective. Matrix metalloproteinase-2 (MMP2) overexpression has been considered as a hallmark of tumor aggressiveness. The significant roles of MMP2 in other human disorders, such as cardiovascular diseases and dental caries, have also been demonstrated. Herein, we used *in silico* approaches to evaluate the binding affinity of selected cinnamic acids to the MMP2 catalytic domain. The obtained findings were subsequently juxtaposed with those attributed to oleandrin, utilized as a reference pharmaceutical agent. **Methods.** This research employed the AutoDock software to assess the affinity of 19 herbal compounds derived from cinnamic acid to the catalytic cleft of MMP2. The ligands attaining the most negative scores, as determined by the Gibbs free binding energy assessments, were accorded the highest rankings. The interactions between the MMP2 and cinnamic acids ranked highest were elucidated using the Discovery Studio Visualizer tool. Molecular dynamics simulations were performed to investigate the structural stability of MMP2 backbone atoms when forming complexes with both the top-ranked inhibitor from this study and a standard drug. **Results.** Eight cinnamic acids were indicated with $\Delta G_{\text{binding}}$ values less than -10 kcal/mol. Cynarin emerged as the most potent inhibitor of the enzyme, with the $\Delta G_{\text{binding}}$ score and inhibition constant value of -15.19 kcal/mol and 7.29 pM, respectively. The MMP2 backbone atoms achieve stability around the 20 ns mark, displaying a root mean square deviation of approximately 3.2 Å when influenced by the top-ranked cinnamic acid, the standard drug, or in their free form. **Conclusion.** The inhibition of MMP2 by cinnamic acids, particularly cynarin, holds promise as a valuable therapeutic strategy for various human disorders, encompassing cancer, cardiovascular conditions, and dental caries.

1. Introduction

Matrix metalloproteinases (MMPs) constitute a family of 23 zinc-dependent endopeptidases primarily responsible for the enzymatic degradation of the extracellular matrix (ECM) [1]. Moreover, they can alter proteins not associated with the ECM, encompassing growth factors, integrins, cadherins, cell surface receptors, and cytokines [2]. MMPs are significantly involved in cell migration, wound healing, bone repair, morphogenesis, tumor invasion, and angiogenesis [3, 4]. MMP2 (gelatinase A), an intrinsic enzyme, can be located in nearly all cellular varieties, and its function

involves the deterioration of denatured collagen (known as gelatin) alongside collagen type IV, in addition to various other ECM proteins [5–7]. MMP2 assumes a pivotal role in facilitating cancer cell invasion by actively participating in the degradation of basement membranes and ECM [8], leading to the metastatic cascade [9]. Gelatinase A is involved in tumor progression, invasion, metastasis, and skeletal dysplasia. In advanced-stage malignancies such as prostate and breast cancers, osteolytic bone metastases are commonly detected, often accompanied by irregular stimulation of MMP2 gene expression [10–12]. Overabundant triggering of MMP2 fosters osteolytic metastasis and

substantial bone deterioration in advanced-stage malignancies [10]. Within breast cancer, there exists a demonstrated association between MMP2 expression and diminished overall survival rates. To illustrate, the mRNA expression levels of MMP2 exhibit a notably elevated status in breast cancer cell lines like MDA-MB-231 and MCF-7 when juxtaposed with the standard HS578Bst cell line [13].

MMP2 expression is elevated in advanced-stage ovarian cancer in contrast to its benign or early-stage counterparts [14]. An earlier meta-analysis revealed that MMP2 was prevalent in a substantial proportion of endometrial cancer cases, and its expression displayed a strong correlation with clinical stage, tumor invasion, and the occurrence of metastasis. This suggests that heightened MMP2 overexpression could potentially function as a prognostic indicator for an unfavorable outcome in endometrial cancer [4]. MMP2 is also involved in several noncancer disorders. For instance, enhanced activity of MMP2 and MMP9 is implicated in various cardiovascular pathological states, such as heart failure, restenosis, atherosclerosis, and ischemic heart disease [15, 16]. In addition, Tjäderhane et al. [17] reported that bacterial acids are required in tooth decay to remove minerals and the subsequent activation of host MMPs, including MMP2, MMP8, and MMP9, leading to dentin matrix degradation. Therefore, Tjäderhane et al. [17] concluded that activating MMPs in human saliva is essential for ultimately destroying the dentin matrix. Karayasheva also reported that MMP2 and MMP3 are likely to be involved in dental caries susceptibility [18].

Natural products have been important sources of new drugs against various pathologies [19]. Cinnamic acid derivatives are within the organic compound category, distinguished by a foundational C6-C3 structure, widely recognized as the phenylpropanoid backbone. The synthesis of these botanical isolates encompasses modifying their aromatic ring and the acrylic acid group, as documented in references [20, 21]. These compounds naturally occur in diverse sources, including cinnamon, coffee beans, olives, fruits, and vegetables [22]. Several cinnamic acid derivatives, including chlorogenic acid, isoferulic acid, caffeic acid, sinapic acid, and ferulic acid, have been shown to possess anti-inflammatory [23–25], antioxidative [26], antitumor [27], cardiovascular [28], and antimicrobial [29] properties. The chemical depiction of cinnamic acid, presented in Figure 1, was created employing ACD/ChemSketch version 12.01.

Historically, traditional approaches to drug discovery have effectively led to the development of novel pharmaceuticals. Still, the journey from identifying a promising lead compound to conducting clinical trials is an extended process, typically exceeding 12 years and incurring an average cost of around USD 1.8 billion. Lately, *in silico* or computer-aided drug design and discovery methodologies have garnered significant attention due to their capacity to expedite the drug development process in terms of time, effort, and expenses. Consequently, this has resulted in the creation of numerous novel pharmaceuticals [30, 31]. Computational drug discovery approaches are based on discovering small molecules that preferentially bind to the

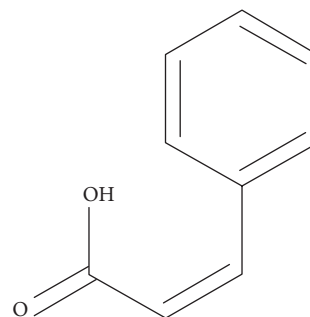


FIGURE 1: Lead scaffold of *cis*-cinnamic acids.

biological target with the highest binding affinity [32]. Due to the several pharmacological effects of cinnamic acids, such as anticancer and anti-inflammatory properties, and the crucial role of MMP2 in tumor development and invasion, this study suggested that cinnamic acid derivatives might be potential MMP2 inhibitors. Therefore, computational drug discovery approaches were conducted to explore cinnamic acids with a high binding affinity to MMP2 and stable interactions within the MMP2 catalytic cleft. The present results may be beneficial in developing new drugs based on herbal compounds for several human disorders, including various cancers, cardiovascular diseases, and dental caries.

2. Materials and Methods

2.1. Structural Preparation of Molecules. The structural information for MMP2 (PDB ID: 1QIB) was acquired from the RCSB database (<https://www.rcsb.org>), with X-ray resolution data available at 2.8 Å [33, 34]. The selection of 1QIB as the focus of our study was based on several considerations. Initially, we directed our attention to the MMP2 page within the UniProt database (<https://www.uniprot.org/uniprotkb/P08253/entry#structure>) [35], specifically emphasizing the 3D structure of the protein. In this context, we opted for the X-ray method. Initially, there were a total of nine PDB IDs in consideration. To refine our selection, we excluded 1GXD due to its comparatively inferior resolution of 3.10 Å. Subsequently, PDB IDs, such as 1CK7, 1EAK, and 3AYU, which represented mutant structures of MMP2, were eliminated from further consideration. Additionally, 1GEN and 1RTG, representing the c-terminal domain of the enzyme and lacking catalytic activity, were also excluded from the study. After this refinement, three PDB IDs—1QIB, 7XGJ, and 7XJI—remained. Notably, 7XGJ and 7XJI contained inhibitors within their files, leading us to speculate that the presence of an inhibitor in the active site might influence the structure of the catalytic domain. Consequently, our choice was narrowed down to 1QIB, the sole PDB ID representing the nonmutant coordination of the MMP2 active site, prepared using the X-ray method and devoid of an inhibitor.

The obtained PDB file included a singular polypeptide chain, designated as chain A, comprising 161 residues. Optimization of the enzyme's structural stability was

achieved through energy minimization using Swiss-PdbViewer (<https://spdbv.unil.ch>). To discern the principal amino acids within the catalytic cleft of MMP2, the interactions between the MMP2 inhibitor (BB94) and the residues at the active site [36] were meticulously examined. The following amino acids were identified as integral components: G-162, L-163, L-164, A-165, V-198, H-201, E-202, P-221, and Y-223. Furthermore, the grid box encompassed Zn-501, Zn-502, Ca-503, Ca-504, and Ca-505.

A curated set comprising 19 cinnamic acids was assembled, and their binding affinities were systematically compared to that of oleandrin (PubChem ID, 11541511; DrugBank ID, 12843), which served as a control inhibitor achieved from the DrugBank repository [37]. During our previous examinations [20, 38, 39], a procedure for energy minimization was executed on the cinnamic acids. PDBQT files were created by modifying the MMP2 structure to incorporate polar hydrogen bonds and Kollman charges. Additionally, rotational motion and local charge were applied to ligands as part of the process. To accomplish this, we made use of MGL tools [40].

2.2. Molecular Docking Analysis. The docking analyses were executed on a Windows-based personal computer equipped with an Intel Core i7 processor, 32 GB of installed RAM, and a 64 bit system architecture [41]. The $\Delta G_{\text{binding}}$ calculation, representing the binding affinities between cinnamic acids, a reference drug, and the MMP2 catalytic cleft, was carried out using the semi-flexible docking approach provided by AutoDock version 4.0 tool [42]. The parameters for the grid box in the docking analysis were configured as follows: X-center, 65.763 Å; Y-center, 31.504 Å; Z-center, 23.821 Å; X-dimension, 60; Y-dimension, 82; and Z-dimension, 86. Each compound generated 50 models to assess the binding affinities with the MMP2 catalytic domain and oleandrin. The docking outcomes underwent clustering with a root mean square (RMS) tolerance of 2.0 Å [40]. Next, the $\Delta G_{\text{binding}}$ value exhibiting the most negative energy within the most significant cluster was chosen for further analysis. Furthermore, interaction mode analysis was generated using the DSV tool.

2.3. Cross-Validation Study. Docking analyses underwent cross-validation for the top-tier cinnamic acids, chosen based on $\Delta G_{\text{binding}}$ values obtained through the AutoDock tool. This validation targeted cinnamic acids, demonstrating a binding energy below -10 kcal/mol within the MMP2 active site. The validation procedure was done using the Schrödinger Maestro docking tool, version 10.2 [43, 44]. The Glide docking system assessed the binding affinity of top-ranked cinnamic acids to the MMP2 catalytic cleft. Within this context, docking values were computed, and the prime MM-GBSA procedure was employed to ascertain the relative binding energies of the compounds. Additional information regarding the configuration parameters in the Schrödinger Maestro docking tool has been documented in a prior investigation conducted by Azadian et al. [45].

2.4. Molecular Dynamics Simulation. Molecular dynamics (MD) examinations were conducted utilizing the Discovery Studio Client tool version 16.1.0.15350, with simulations extending for 100 nanoseconds (ns) on unfettered MMP2 and in conjunction with the top-rated inhibitor identified in this research, along with oleandrin as a standard drug. A 64 bit system architecture, 64 GB of DDR5 installed memory, and an Intel 24-Core i9-13900KF processor were utilized for the MD simulations, which boasted a more potent computer setup than the docking analyses. The advanced parameters for computer simulations, such as the solvent type, solvation model, force field, cell geometry, and final temperature, were determined based on our prior investigations [41, 46]. Various assessments, including the root mean square fluctuation (RMSF) and root mean square deviation (RMSD) of MMP2's backbone atoms, total energy, and radius of gyration (ROG) of protein during the simulation period, were conducted using MD simulations [47].

Ensuring the robustness of the MD simulations, with a focus on MMP2 backbone atoms during a 100 ns trajectory, involved various validation measures. An equilibration phase was initiated before the production MD run, where the system attained a stable state by applying positional restraints. The system was gradually heated to the desired temperature (310 K), followed by a gradual pressure equilibration. The selection of a reliable force field (CHARMM) [48], recognized for its precision in capturing biomolecular behavior, was undertaken, ensuring compatibility with the parameters of the ligands and the MMP2 protein. Oleandrin, functioning as a standard drug, provided a benchmark for the dynamics of MMP2-oleandrin in our simulations, facilitating comparisons with the behavior of free MMP2 and MMP2 complexed with the top-ranked cinnamic acid. Key parameters, including RMSD, ROG, and total energy, were monitored throughout the simulation to gain insights into the system's convergence.

2.5. Pharmacokinetics of Cinnamic Acids. The assessment of the absorption, distribution, metabolism, and excretion (ADME) of cinnamic acids was conducted using the SwissADME web server, available at (<https://www.swissadme.ch/>) [49]. Various pharmacokinetic parameters of the compounds were considered within the ADME framework, encompassing gastrointestinal absorption, blood-brain barrier permeability, potential cytochrome P-450 inhibition, and susceptibility as a substrate for P-glycoprotein.

3. Results

3.1. Binding Affinities Based on AutoDock. According to the results, a total of eight cinnamic acid derivatives, including cynarin, rosmarinic acid, chlorogenic acid, caffeic acid 3-glucoside, caffeic acid phenethyl ester, phenethyl caffeate, cinnamyl caffeate, and benzyl caffeate, exhibited $\Delta G_{\text{binding}}$ scores less than -10 kcal/mol and considered as top-ranked MMP2 inhibitors. Among these, cynarin, rosmarinic acid, and chlorogenic acid were found to reduce the enzyme's

activity in the picomolar concentration. Cynarin emerged as the most powerful MMP2 inhibitor in this investigation. This ligand attached to the MMP2 catalytic cleft with the $\Delta G_{\text{binding}}$ score and K_i value of -15.19 kcal/mol and 7.29 Pm, respectively. The $\Delta G_{\text{binding}}$ score of -8.8 kcal/mol between MMP2 and oleandrin was identified. Consequently, all top-ranked cinnamic acids and roscovitine demonstrated greater affinity to the MMP2 catalytic cleft compared to the control inhibitor. Table 1 provides the affinities between cinnamic acids, oleandrin, and MMP2, displaying the calculated $\Delta G_{\text{binding}}$ and K_i values between the enzyme and compounds. Additionally, Table 2 provides a comprehensive analysis of all energy values calculated between the MMP2 active site and the cinnamic acids ranked highest in our findings. Figure 2 compares the binding affinities between the most potent MMP2 inhibitors, oleandrin, and the enzyme's catalytic cleft.

3.2. Cross-Validations. The Schrödinger Maestro computed docking scores for cynarin, rosmarinic acid, and chlorogenic acid. G scores (docking scores) revealed that rosmarinic acid displayed the most affinity to the MMP2 catalytic domain, securing the highest rank among the compounds, followed by cynarin and chlorogenic acid. Additionally, according to MM-GBSA binding energies in Table 3, cynarin emerged as the most potent MMP2 inhibitor, followed by rosmarinic acid and chlorogenic acid.

The results from both AutoDock 4.0 and Schrödinger Maestro concurred in identifying cynarin's notable binding affinity to the MMP2 catalytic cleft, justifying its selection for subsequent MD analysis. Notably, MD analyses were conducted utilizing the docking outcomes from the AutoDock tool.

3.3. MMP2 Stability. The RMSF plots indicate reduced fluctuations in the active site of MMP2 when obstructed by oleandrin and cynarin compared to its unbound state (Figure 3(a)). Consequently, it is presumed that the most potent inhibitor of MMP2 in this investigation provided greater stabilization to gelatinase A than the free protein. Per the RMSD plot, the receptor exhibited enhanced stability when bound to cynarin, surpassing its unbound state. Notably, the greatest stability was observed when the standard drug blocked MMP2. According to the information in Figure 3(b), the protein's backbone atoms achieve stability around the 20 ns mark, with an RMSD of roughly 3.2 Å when hindered by cynarin, oleandrin, or in its free form. During the 100 ns MD simulation, the ROG values for MMP2, MMP2–oleandrin, and MMP2–cynarin exhibited oscillatory changes.

Interestingly, the ROG value of the MMP2–cynarin complex was lower than that of free MMP2 throughout the simulation, as shown in Figure 4(a). Besides, the MMP2–oleandrin complex demonstrated the lowest ROG value throughout the entire simulation. By the MD simulation results in Figure 4(b), the enzyme's total energy

complexed with cynarin was lower than that of MMP2 and MMP2–oleandrin. Figure 5 visually presents the superimposed coordinates of free MMP2, MMP2 blocked by cynarin, and oleandrin before and after computer simulations, as observed using the DSV tool. Furthermore, the incorporation of cynarin into the gelatinase A active site was demonstrated using DSV in the hydrophobicity surface mode, both before and following MD simulation, as depicted in Figure 6.

3.4. Interaction Modes. Through the DSV tool, it was possible to reveal the interactions between oleandrin, the highest-ranked MMP2 inhibitor, and the residues within the active site of the enzyme. Among the scrutinized cinnamic acids, rosmarinic acid established the highest number of hydrogen bonds ($n=6$), while caffeic acid phenethyl ester engaged in the most hydrophobic interactions ($n=4$) with the enzyme's active site. Before MD simulation, cynarin formed two H-bonds and two hydrophobic interactions with MMP2. Subsequently, following MD simulation, cynarin established one H-bond with the receptor. Before MD simulation, oleandrin engaged in one hydrogen bond and nine hydrophobic interactions with the receptor's active site.

Furthermore, oleandrin exhibited three H-bonds and five hydrophobic interactions with amino acids inside the MMP2 active site. The chemical connections between the foremost cinnamic acids, oleandrin, and the MMP2 active site are comprehensively displayed in Table 4, excluding hydrogen bonds that had distances exceeding 5 Å. In addition, Supplementary Figure 1 provides a two-dimensional view of the docked poses of cynarin, rosmarinic acid, chlorogenic acid, and oleandrin, within the MMP2 catalytic cleft.

3.5. ADME Prediction. As detailed in Table 5, the ADMET prediction study reveals distinctive characteristics among the examined compounds. Cynarin, rosmarinic acid, chlorogenic acid, and caffeic acid 3-glucoside were identified as having a reduced level of gastrointestinal absorbance. In contrast, other cinnamic acid derivatives exhibited a comparatively higher absorption in the gastrointestinal tract. Furthermore, cynarin, rosmarinic acid, chlorogenic acid, caffeic acid 3-glucoside, roscovitine, caffeic acid, and sinapinic acid demonstrated a notable absence of blood–brain barrier permeability, in contrast to the remaining compounds that exhibited permeability through the blood–brain barrier. Regarding susceptibility as a substrate for P-glycoprotein, SwissADME predictions highlighted that cynarin and roscovitine have the potential to bind to P-glycoprotein, indicating a possible risk of inducing drug resistance. Additionally, phenethyl caffeate, cinnamyl caffeate, roscovitine, artemillin C, and N-p-coumaroyltyramine displayed inhibitory effects against at least one cytochrome P-450, suggesting potential challenges in drug excretion. Conversely, the remaining compounds were anticipated to undergo facile excretion from the body.

TABLE 1: The K_i values and Gibbs free energies were determined for the interactions between gelatinase A, 19 cinnamic acids, and oleandrin, which served as the control inhibitor.

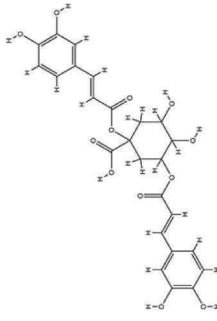
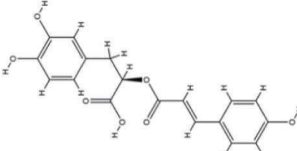
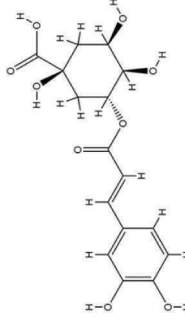
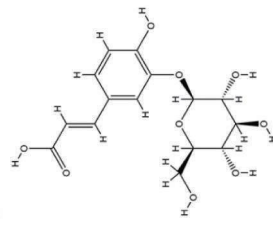
PubChem ID	Cinnamic acids	$\Delta G_{\text{binding}}$ (kcal/mol)	Inhibition constant	Chemical structure
6124212	Cynarin	-15.19	7.29 pM	
5281792	Rosmarinic acid	-13.56	115.25 pM	
1794427	Chlorogenic acid	-12.81	409.21 pM	
5281759	Caffeic acid 3-glucoside	-10.93	9.76 nM	

TABLE 1: Continued.

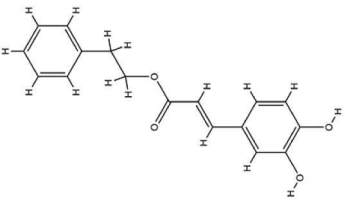
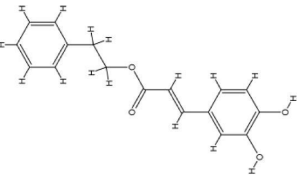
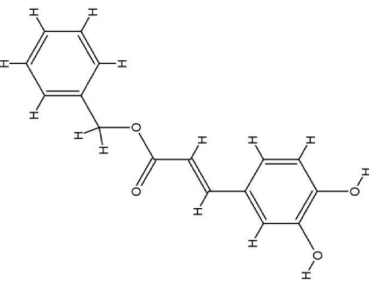
PubChem ID	Cinnamic acids	$\Delta G_{\text{binding}}$ (kcal/mol)	Inhibition constant	Chemical structure
5281787	Caffeic acid phenethyl ester (phenethyl caffeate)	-10.54	18.79 nM	
11380911	Cinnamyl caffeate	-10.46	21.39 nM	
5919576	Benzyl caffeate	-10.28	29.34 nM	

TABLE 1: Continued.

PubChem ID	Cinnamic acids	$\Delta G_{\text{binding}}$ (kcal/mol)	Inhibition constant	Chemical structure
160355	Roscovitine	-9.81	64.56 nM	
5472440	Artepillin C	-8.45	638.97 nM	
689043	Caffeic acid	-7.98	1.41 uM	
637540	o-Coumaric acid	-7.94	1.52 uM	

TABLE 1: Continued.

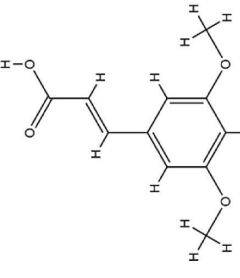
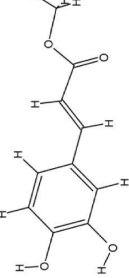
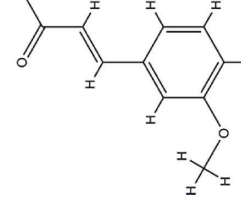
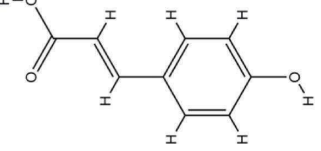
PubChem ID	Cinnamic acids	$\Delta G_{\text{binding}}$ (kcal/mol)	Inhibition constant	Chemical structure
637775	Sinapinic acid	-7.79	1.95 μM	
689075	Methyl caffeate	-7.74	2.12 μM	
445858	Ferulic acid	-7.31	4.35 μM	
637542	p-Coumaric acid	-6.88	9.04 μM	

TABLE 1: Continued.

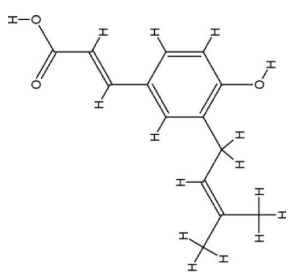
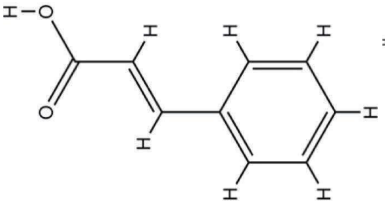
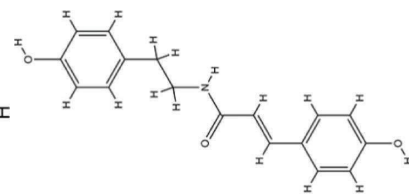
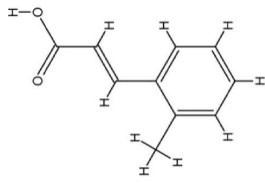
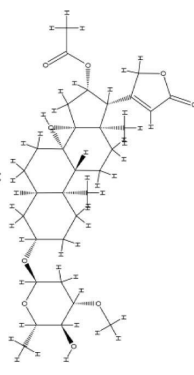
PubChem ID	Cinnamic acids	$\Delta G_{\text{binding}}$ (kcal/mol)	Inhibition constant	Chemical structure
6440361	Drupanin	-6.68	12.76 μM	
444539	<i>trans</i> -Cinnamic acid	-6.17	30.23 μM	
5372945	N-p-coumaroyltyramine	-5.76	59.68 μM	

TABLE 1: Continued.

PubChem ID	Cinnamic acids	$\Delta G_{\text{binding}}$ (kcal/mol)	Inhibition constant	Chemical structure
819020	2-Methylcinnamic acid	-5.49	94.99 μM	
11541511	Oleandrin (Ctrl+)	-8.8	354.37 nM	

K_i , inhibition constant; Ctrl, control.

TABLE 2: Different energies between top-ranked cinnamic acids, oleandrin, and MMP2 catalytic cleft.

Top-ranked cinnamic acids	Final intermolecular energy (kcal/mol)	Final total internal energy (kcal/mol)	Torsional free energy (kcal/mol)	Unbound system's energy (kcal/mol)	Estimated free energy of binding (kcal/mol)
Cynarin	-4.56	-18.97	6.26	-2.07	-15.19
Rosmarinic	-10.83	-8.21	4.47	-1.01	-13.56
Chlorogenic acid	-8.56	-9.93	4.18	-1.51	-12.81
Caffeic acid 3-glucoside	-10.78	-5.22	3.88	-1.19	-10.93
Caffeic acid phenethyl ester	-11.81	-2.17	2.98	-0.45	-10.54
Phenethyl caffeate	-11.12	-2.29	2.39	-0.53	-10.49
Cinnamyl caffeate	-11.57	-1.8	2.39	-0.51	-10.46
Benzyl caffeate	-10.48	-1.9	1.49	-0.62	-10.28
Oleandrin (Ctrl+)	-9.76	-2.95	2.39	-1.53	-8.8

MMP2, matrix metalloproteinase-2.

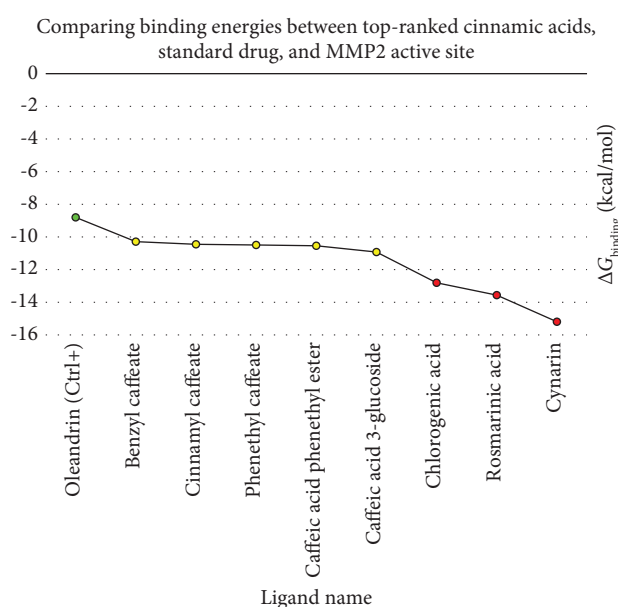


FIGURE 2: The $\Delta G_{\text{binding}}$ values depict the Gibbs free energy of binding, expressed in kcal/mol units, corresponding to the interactions between the MMP2 active site, the enzyme's control inhibitor, and the cinnamic acids ranked highest. The names of the ligands can be found on the X-axis, while the Y-axis represents the corresponding Gibbs free binding energy values. A green diamond denotes the reference drug, and the most potent inhibitors of gelatinase A are depicted by red spots with a K_i value in the picomolar scale. Yellow spots highlight the additional cinnamic acids with K_i values in the nanomolar range. MMP2, matrix metalloproteinase-2; K_i , inhibition constant.

TABLE 3: Schrödinger Maestro docking scores and relative binding-free energies obtained by prime MM-GBSA (kcal/mol) of top-ranked cinnamic acids based on the AutoDock tool against MMP2 active site (PDB ID, 1QIB).

Compound name	G score	MM-GBSA-dG binding energy
Cynarin	-9.77	-26.95
Rosmarinic acid	-11	-24.79
Chlorogenic acid	-8.76	-20.72

MMP2, matrix metalloproteinase-2.

4. Discussion

The biological roles and expression levels of MMP2 have been intensively studied. Its heightened presence in nearly all malignancies was viewed as a distinctive sign of cancer's aggressiveness, spurring research efforts focused on

restraining it [50]. The significant roles of MMP2 in several cardiovascular disorders [15, 16] and dental caries have also been demonstrated [17, 18].

The present study evaluated the affinity of several cinnamic acids to the MMP2 catalytic cleft to discover potential inhibitors of MMP2 from cinnamic acids. The AutoDock

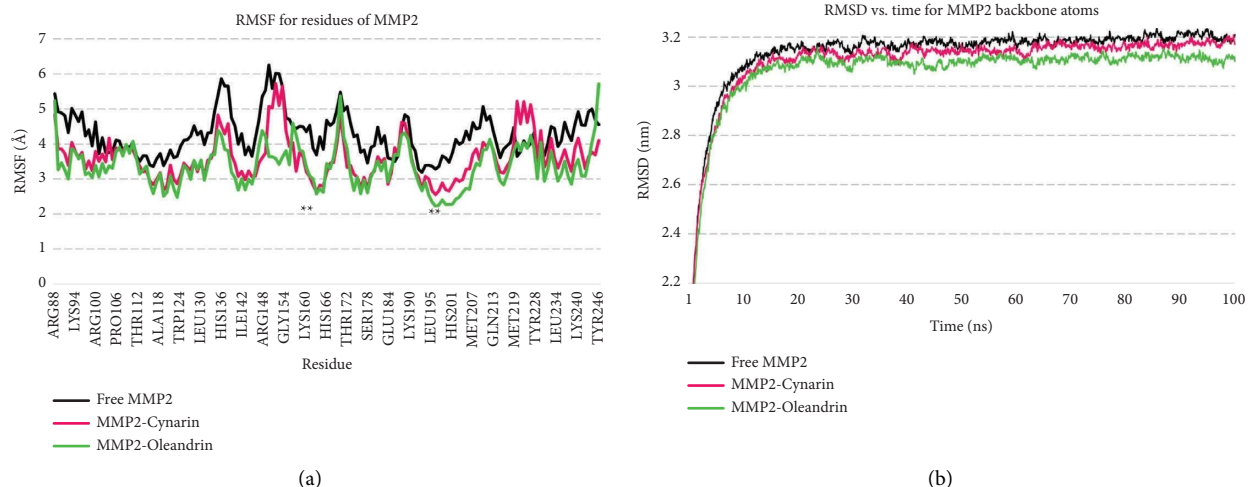


FIGURE 3: The impact of free MMP2 backbone atoms during a 100 ns MD simulation was studied with a focus on (a) RMSF and (b) RMSD to examine the influence of cynarin and oleandrin. The asterisks in the RMSF plots denote the active site of the receptor. MMP2, matrix metalloproteinase 2; RMSF, root mean square fluctuation; RMSD, root mean square deviations.

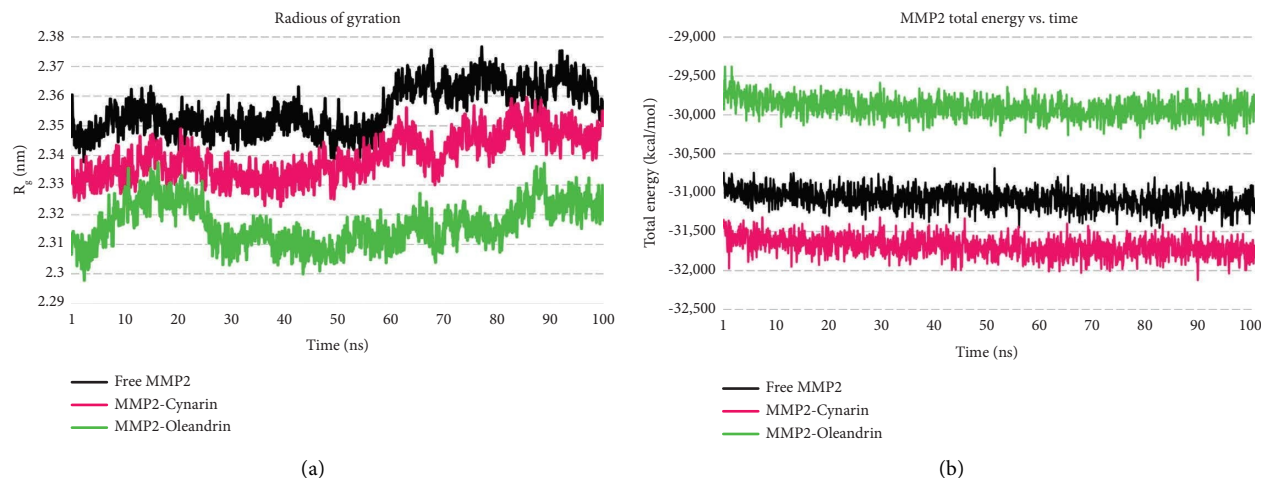


FIGURE 4: The study investigated the impact of free MMP2 backbone atoms during a 100 ns MD simulation, with a specific emphasis on (a) ROG and (b) total energy plots. The objective was to scrutinize the influence of cynarin and oleandrin on these two parameters. MMP2, matrix metalloproteinase 2; MD, molecular dynamics; ROG, radius of gyration.

tool indicated that eight cinnamic acids had considerable binding affinities to the gelatinase A active site ($\Delta G_{\text{binding}} < -10$ kcal/mol), in which cynarin, rosmarinic acid, and chlorogenic acid demonstrated salient binding affinities with the $\Delta G_{\text{binding}}$ value of -15.19 , -13.56 , and -12.81 kcal/mol, respectively. The Schrödinger Maestro has substantiated the pronounced binding affinity observed among cynarin, rosmarinic acid, chlorogenic acid, and MMP2.

4.1. Primary Sources and Pharmacodynamics of Leading Compounds. Cynarine represents one of the prominent caffeoylquinic acid constituents derived from the artichoke (*Cynara scolymus* L.) [51]. Cynarin formed two hydrogen

and two hydrophobic interactions with Asp161, Gly162, Ile222, and Tyr223 within the gelatinase A active site before MD simulation. Besides, only one hydrogen bond with Asp161 was observed for this compound after MD simulation, and this bond was found to remain stable throughout the 100 ns computer simulation.

Chlorogenic acid is predominantly encountered in traditional Chinese medicinal plants, such as honeysuckle, hawthorn, eucommia, and chrysanthemum, and is particularly abundant in coffee [52]. Chlorogenic acid illustrated five hydrogen bonds with Leu218 and Thy227 incorporated inside the enzyme's active site.

Rosmarinic acid is a flavonoid frequently encountered in *Perilla frutescens* (L.) Britton, *Rosmarinus officinalis* L., and *Melissa officinalis* L., commonly present in teas, culinary

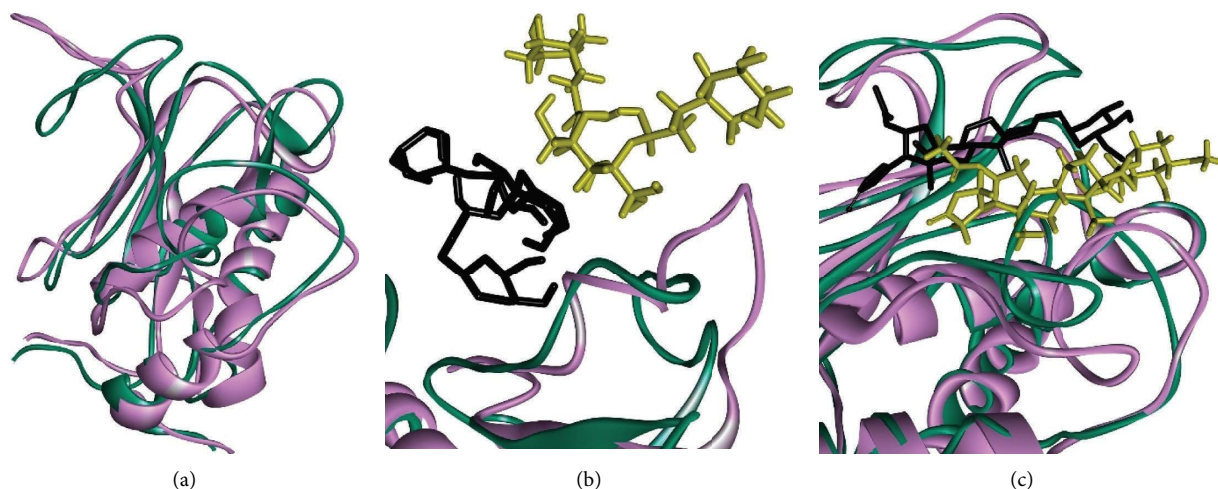


FIGURE 5: Following a 100 ns MD simulation, the superimposition of structures was performed for (a) free MMP2, (b) MMP2 with cynarin, and (c) MMP2 with oleandrin. The protein chains were depicted in green and purple to indicate their states before and after the MD analysis. Additionally, the ligands were portrayed in black and yellow to represent their conditions before and after the MD simulations. MMP2, matrix metalloproteinase 2; MD, molecular dynamics.

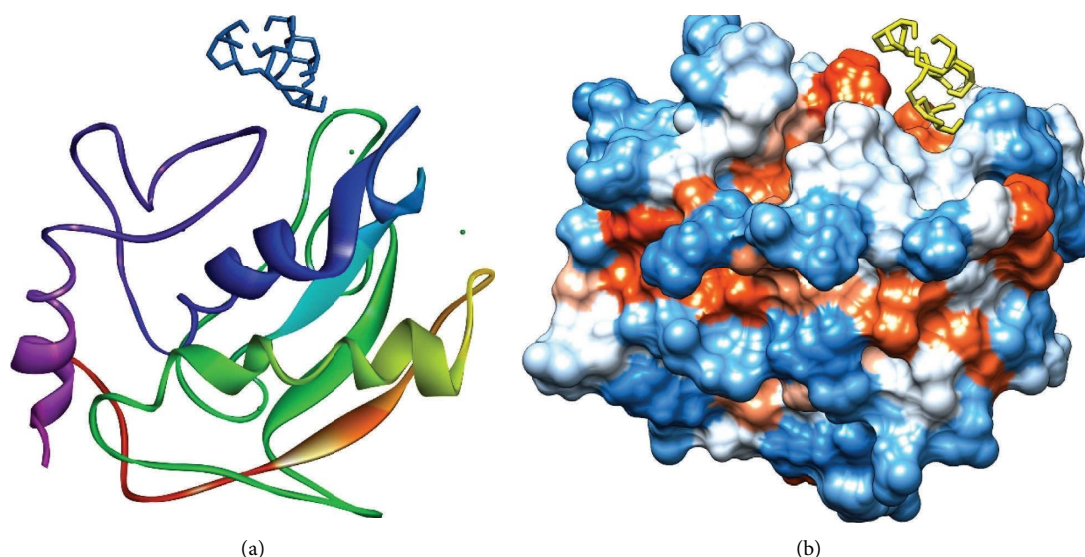


FIGURE 6: The 3D depiction of MMP2 was presented when the enzyme's active site was blocked by cynarin in (a) ribbon and (b) hydrophobicity surface mode. MMP2, matrix metalloproteinase 2; MD, molecular dynamics.

TABLE 4: The interaction modes between the MMP2 catalytic cleft, the highest-ranked cinnamic acids, and oleandrin as a positive control inhibitor.

Ligand name	Hydrogen bonds (distance Å)	Hydrophobic interactions (distance Å)
Cynarin (before MD)	Gly162 (3.60); Asp161 (3.11)	Ile222 (5.28); Tyr223 (5.08)
Cynarin (after MD)	Asp161 (3.59)	NA
Rosmarinic acid	Leu218 (3.62); Thr227 (3.54,3.68); Pro215 (4.69); Leu197 (3.94, 4.50)	His201 (5.98)
Chlorogenic acid	Thr227 (2.73, 3.21, 4.07); Leu218 (4.26, 3.39)	NA
Caffeic acid 3-glucoside	Thr229 (3.87); Thr227 (4.59); Pro215 (4.80); Ala217 (3.56); Glu202 (4.56)	His201 (5.39); Val198 (5.03); Leu218 (5.90)
Caffeic acid phenethyl ester	Thr227 (3.62, 2.77, 4.02)	Val198 (3.65); His201 (3.77); Leu164 (6.11); Ala220 (4.45)

TABLE 4: Continued.

Ligand name	Hydrogen bonds (distance Å)	Hydrophobic interactions (distance Å)
Phenethyl caffeate	Glu202 (4.66); Thr227 (4.75)	Ala220 (5.82); Val198 (4.35)
Cinnamyl caffeate	Glu202 (4.63); Thr223 (4.47)	Val198(4.07); Phe232 (5.76); Leu218 (4.37)
Benzyl caffeate	Glu202 (4.77); Thr227 (4.84)	Ala220 (6.08); Val198 (4.14)
Oleandrin (Ctrl+) (before MD)	Tyr223 (4.23)	Ile222 (5.07); Leu164 (4.01, 4.7); Leu163 (3.83, 4.93, 5.79); His211 (6.78); His201 (6.02); His205 (5.28)
Oleandrin (Ctrl+) (after MD)	Glu210 (3.8); Pro221 (4.35); Tyr223 (4.98)	His205 (6.15, 7.03); His201 (7.37); Tyr193 (4.95); Tyr223 (5.88)

MMP2, matrix metalloproteinase-2; Ctrl, control.

TABLE 5: Predicted ADME for cinnamic acids in this study.

Ligand name	GI abs	BBB permeant	P-gp substrate	CYP1A2 inhibitor	CYP2C19 inhibitor	CYP2C9 inhibitor	CYP2D6 inhibitor	CYP3A4 inhibitor
Cynarin	Low	No	Yes	No	No	No	No	No
Rosmarinic acid	Low	No	No	No	No	No	No	No
Chlorogenic acid	Low	No	No	No	No	No	No	No
Caffeic acid 3-glucoside	Low	No	No	No	No	No	No	No
Caffeic acid phenethyl ester (phenethyl caffeate)	High	Yes	No	Yes	No	Yes	No	No
Cinnamyl caffeate	High	Yes	No	Yes	No	Yes	No	No
Benzyl caffeate	High	Yes	No	No	No	No	No	No
Roscovitine	High	No	Yes	Yes	No	No	Yes	Yes
Artepillin C	High	Yes	No	No	Yes	Yes	No	No
Caffeic acid	High	No	No	No	No	No	No	No
o-Coumaric acid	High	Yes	No	No	No	No	No	No
Sinapinic acid	High	No	No	No	No	No	No	No
Methyl caffeate	High	Yes	No	No	No	No	No	No
Ferulic acid	High	Yes	No	No	No	No	No	No
p-Coumaric acid	High	Yes	No	No	No	No	No	No
Drupanin	High	Yes	No	No	No	No	No	No
Cinnamic acid	High	Yes	No	No	No	No	No	No
N-p-coumaroyltyramine	High	Yes	No	No	No	No	Yes	Yes
2-Methylcinnamic acid	High	Yes	No	No	No	No	Yes	Yes

GI, gastrointestinal; abs, absorption; BBB, blood-brain barrier; P-gp, P-glycoprotein; CYP, cytochrome p-450.

seasonings, and spices. The extensive utilization of rosmarinic acid for health enhancement is attributed to its potent antioxidant capabilities [53, 54]. Rosmarinic acid demonstrated six H-bonds and one hydrophobic interaction with Leu197, His201, Pro215, Leu218, and Thr227 inside the gelatinase A catalytic cleft.

4.2. Structure-Activity Relationship. Examining the $\Delta G_{\text{binding}}$ values between the assessed cinnamic acids and the MMP2 active site can provide insights into these compounds' structure-activity relationship (SAR), potentially contributing valuable information to cancer drug design. Based on the current data, a hypothesis emerges, suggesting that cinnamic acid derivatives with two C6 rings, such as cynarin, rosmarinic acid, caffeic acid phenethyl ester, cinnamyl caffeate, and benzyl caffeate, or those with a single benzene ring accompanied by a sugar moiety, like caffeic acid 3-glucoside, exhibit a stronger binding affinity compared to those with only a single C6 ring, such as 2-methylcinnamic acid,

cinnamic acid, drupanin, p-coumaric acid, ferulic acid, methyl caffeate, sinapinic acid, o-coumaric acid, caffeic acid, and artepillin C.

An exception to this trend is N-p-coumaroyltyramine, which, despite featuring two C6 rings, demonstrates a low binding affinity to MMP2 with a $\Delta G_{\text{binding}}$ value of -5.76 kcal/mol. Notably, chlorogenic acid, comprising a phenolic acid core, quinic acid, and an ester linkage, is structurally distinct. Although quinic acid is not a true sugar, being a polyhydroxy carboxylic acid, its presence in chlorogenic acid contributes to elements resembling sugar moieties. This structural feature results in a high binding affinity to MMP2, as evidenced by a $\Delta G_{\text{binding}}$ value of -12.81 kcal/mol.

In the context of ADME properties, the following SARs are suggested for cinnamic acid derivatives:

4.2.1. Gastrointestinal Absorption. Smaller cinnamic acids, such as 2-methylcinnamic acid, cinnamic acid, drupanin, p-coumaric acid, ferulic acid, methyl caffeate, sinapinic acid, o-

coumaric acid, caffeic acid, and artemillin C, are predicted to exhibit higher gastrointestinal absorption compared to larger ones like cynarin, rosmarinic acid, chlorogenic acid, and caffeic acid 3-glucoside.

4.2.2. BBB Permeability. Smaller compounds, such as 2-methylcinnamic acid, cinnamic acid, drupanin, p-coumaric acid, ferulic acid, methyl caffeate, o-coumaric acid, and artemillin C, demonstrate greater permeability through the BBB compared to larger cinnamic acids, including cynarin, rosmarinic acid, chlorogenic acid, caffeic acid 3-glucoside, and roscovitines.

These observations suggest that the size of the cinnamic acid derivatives plays a significant role in their ADME characteristics, with smaller compounds generally showing more favorable properties in terms of gastrointestinal absorption and BBB permeability.

4.3. Comparing the Results with the Literature. In a previous study performed by Malekipour et al. [39], considerable binding affinities were also observed among cynarin, rosmarinic acid, chlorogenic acid, and MMP9 active site with $\Delta G_{\text{binding}}$ values of -14.68 , -11.85 , and -12.62 kcal/mol, respectively. The results of the study by Malekipour et al. [39] were consistent with our findings, demonstrating the potential of cinnamic acid derivatives in blocking gelatinase A and B active sites.

A previous report by Hajiaghaee et al. [55] indicated that the aerial parts of *Scrophularia striata* Boiss (*S. striata*) have inhibitory effects against the activity and/or expression of MMP2 and MMP9 in a fibrosarcoma cell line (WEHI-164). However, the herbal isolates of *S. striata* were not demonstrated then. A few years later, Monsef-Esfahani et al. [56] performed an experimental study using chromatography and proton nuclear magnetic resonance (^1H NMR) techniques to unravel chemical compounds isolated from *S. striata*. The authors extracted five active compounds from the *S. striata*, one of which was demonstrated to be cinnamic acid, suggesting its potential role in inhibiting MMP2 and MMP9.

Yen et al. [57] subjected human adenocarcinoma A549 cells to varying concentrations (ranging from 0 to 200 μM) of *cis*-cinnamic acid and *trans*-cinnamic acid while exposed to 200 nM phorbol-12-myristate-13-acetate (PMA) at 37°C for 24 hours. Subsequently, they assessed the activities of MMP2 and MMP9, adhesive properties, migratory capabilities, and invasive behaviors of these cells. In their study, Yen et al. [57] documented that administering *cis*-cinnamic acid and *trans*-cinnamic acid led to a dose-dependent decline in the PMA-induced activities of MMP2 and MMP9. Furthermore, the PMA-triggered mobility was inhibited in a manner directly proportional to the dosage during the 24-hour exposure to *cis*-cinnamic acid and *trans*-cinnamic acid. The capacity for invasion exhibited a noteworthy reduction, reaching 68% and 65%, respectively, indicating that both *cis*-cinnamic acid and *trans*-cinnamic

acid act as inhibitors of A549 cell invasion. Notably, the inhibitory effect of *cis*-cinnamic acid appears to surpass that of *trans*-cinnamic acid.

Keskin et al. [58] synthesized silver nanoparticles (AgNPs) using the aqueous solution of leaf extract derived from *Diospyros kaki* L. (*D. Kaki*). The researchers also employed liquid chromatography-tandem mass spectrometry to scrutinize the chemical makeup of the *D. kaki* leaf extract, to identify potential biologically active components. As per the findings from the research conducted by Keskin et al. [58], the *D. kaki* leaf extract exhibited the highest concentrations of cynarin, chlorogenic acid, quercetin-3-D-xyloside, hyperoside, and quercetin-3-glucoside, in that respective order. Moreover, in their study, Keskin et al. [58] executed the MTT assay to study the cytotoxic impact of the synthesized AgNPs on various cancer cell lines, which included human ovarian sarcoma Skov-3, human colorectal adenocarcinoma Caco-2, glioblastoma U118, and the human dermal fibroblast (HDF) healthy cell line. The researchers illustrated that the DK-AgNPs exhibited an inhibitory influence on the growth of the cancer cell lines. The outcomes of the study by Keskin et al. [58] validate the *in vitro* anticancer properties of cynarin and chlorogenic acid.

Zhao et al. [59] conducted a comprehensive review outlining the antineoplastic potential of rosmarinic acid across diverse cancer types and its role in enhancing chemoradiotherapy sensitivity. As an illustration, rosmarinic acid effectively curbed the expression of MMP2 and MMP9 and the invasive capabilities of multiple tumor cell lines. Additionally, it demonstrated a mitigating effect on lung metastasis in a mouse model of colorectal cancer [60, 61]. By functioning as a Fyn inhibitor, rosmarinic acid displayed its ability to downregulate MMP2 and MMP9, suppressing tumor invasion and migration. This effect was observed in treating both hepatocellular carcinoma and glioma [62]. The inhibition of AKT phosphorylation and the concurrent repression of MMPs played a pivotal role in diminishing the tumor's invasive capabilities. This phenomenon was observed in studies referenced as [63, 64]. Research has indicated that rosmarinic acid had the effect of upregulating miRNAs, specifically miR-506 and miR-1225-5p. These miRNAs targeted the MMPs 3'untranslated regions, inhibiting epithelial-to-mesenchymal (ETM) transition and consequently suppressing tumor metastasis. This information was derived from studies cited as [65, 66].

4.4. Antitooth Caries Properties of Top-Ranked Compounds. Mojtabavi et al. [67] documented that the combination of cinnamic acid (at a concentration of 10 mM) and laccase (at a concentration of 0.125 U·ml⁻¹) resulted in a notable reduction, approximately 90% in the formation of *Streptococcus mutans* (*S. mutans*) biofilms. *S. mutans* stands out as the most prominent and widespread species among the bacterial pathogens responsible for causing dental caries [68]. Ferrazzano et al. [69] showed that chlorogenic acid disrupted the adhesion of *S. mutans* to hydroxyapatite beads coated with saliva. Koo et al. [70] conveyed that ethanolic

propolis extracts from Northeastern Brazil, encompassing p-coumaric acid, exhibited significant biological activity against *S. mutans*. Saleh et al. [71] recently published findings indicating the presence of elevated concentrations of chlorogenic and caffeic acids in propolis extract, as determined through high-performance liquid chromatography (HPLC). The researchers showcased that propolis extracts, as well as propolis extract-functionalized hydrogels, displayed promising antimicrobial properties against various bacteria, including *S. mutans*.

5. Conclusion

The current investigation implies that cynarin, rosmarinic acid, chlorogenic acid, caffeic acid 3-glucoside, caffeic acid phenethyl ester, phenethyl caffeate, cinnamyl caffeate, and benzyl caffeate exhibit substantial binding affinities toward the active site of MMP2. Among these metabolites, cynarin, rosmarinic acid, and chlorogenic acid demonstrated inhibition constant scores at the picomolar range. Utilizing AutoDock, the $\Delta G_{\text{binding}}$ values for cynarin, rosmarinic acid, and chlorogenic acid binding to the MMP2 catalytic cleft were determined as -15.19 , -13.56 , and -12.82 kcal/mol, respectively. Additionally, employing Schrödinger, the MM-GBSA scores computed for these botanical isolates interacting with MMP2 were -26.95 , -24.79 , and -20.72 kcal/mol. Notably, these results from Schrödinger align with the findings obtained through AutoDock. After a 100 ns computer simulation, a stable hydrogen bond was identified between cynarin and Asp161. Moreover, the MMP2 backbone atoms reach a state of stability at approximately the 20 ns mark, exhibiting an RMSD of 3.2 Å, whether influenced by cynarin, oleandrin, or in their free state. These discoveries could provide valuable insights to scientists who aspire to develop new drug therapies for various conditions, including malignancy, cardiovascular disorders, and dental caries. Nevertheless, further investigations are necessary to validate the current findings, encompassing both *in vitro* and *in vivo* validation experiments.

Data Availability

The datasets used and/or analyzed during the current study are available from the corresponding author upon reasonable request.

Ethical Approval

The present study has been confirmed by the Ethics Committee of Hamadan University of Medical Sciences, Hamadan, Iran (IR.UMSHA.REC.1401.569).

Conflicts of Interest

The authors declare that they have no conflicts of interest.

Authors' Contributions

AT and SS designed the study. MRZ and ZA performed AutoDock and Schrödinger Maestro docking tools, respectively. MD simulations were executed by AT. AT, SS, and SJ analyzed and discussed the results. AT wrote the manuscript. SS and SJ edited the manuscript. All authors read and approved the final version of the manuscript.

Acknowledgments

The authors acknowledge the support of the Deputy of Research and Technology, Research Center for Molecular Medicine, and Dental Research Center, Hamadan University of Medical Sciences, Hamadan, Iran.

Supplementary Materials

Supplementary Figure 1: A two-dimensional visual representation showcases the highest-ranked cinnamic acids and the reference drug within the active site of MMP2. Specifically, panels (a) and (b) illustrate cynarin before and after the molecular dynamics (MD) simulation, respectively. Panels (c) and (d) present oleandrin before and after the MD simulation, while panels (e) and (f) also feature rosmarinic acid and chlorogenic acid, respectively. MMP2, matrix metalloproteinase-2. (*Supplementary Materials*)

References

- [1] H. Nagase and J. F. Woessner, "Matrix metalloproteinases," *Journal of Biological Chemistry*, vol. 274, no. 31, pp. 21491–21494, 1999.
- [2] C. M. Overall and C. López-Otín, "Strategies for MMP inhibition in cancer: innovations for the post-trial era," *Nature Reviews Cancer*, vol. 2, no. 9, pp. 657–672, 2002.
- [3] G. Sawicki, "Intracellular regulation of matrix metalloproteinase-2 activity: new strategies in treatment and protection of heart subjected to oxidative stress," *Scientific*, vol. 2013, pp. 130451–12, 2013.
- [4] C. Liu, Y. Li, S. Hu et al., "Clinical significance of matrix metalloproteinase-2 in endometrial cancer: a systematic review and meta-analysis," *Medicine*, vol. 97, no. 29, pp. 191–208, 2018.
- [5] H. Birkedal-Hansen, W. G. Moore, M. K. Bodden et al., "Matrix metalloproteinases: a review," *Critical Reviews in Oral Biology & Medicine: An Official Publication of the American Association of Oral Biologists*, vol. 4, no. 2, pp. 197–250, 1993.
- [6] S. Löffek, O. Schilling, and C. W. Franzke, "Biological role of matrix metalloproteinases: a critical balance," *European Respiratory Journal*, vol. 38, no. 1, pp. 191–208, 2011.
- [7] C. J. Morrison, G. S. Butler, D. Rodríguez, and C. M. Overall, "Matrix metalloproteinase proteomics: substrates, targets, and therapy," *Current Opinion in Cell Biology*, vol. 21, no. 5, pp. 645–653, 2009.
- [8] Z. Fu, S. Xu, Y. Xu, J. Ma, J. Li, and P. Xu, "The expression of tumor-derived and stromal-derived matrix metalloproteinase 2 predicted prognosis of ovarian cancer," *International Journal of Gynecological Cancer*, vol. 25, no. 3, pp. 356–362, 2015.

- [9] M. Tauro and C. C. Lynch, "Cutting to the chase: how matrix metalloproteinase-2 activity controls breast-cancer-to-bone metastasis," *Cancers*, vol. 10, no. 6, p. 185, 2018.
- [10] P. Reveglia, C. Paolillo, G. Ferretti et al., "Challenges in LC-MS-based metabolomics for Alzheimer's disease early detection: targeted approaches versus untargeted approaches," *Metabolomics*, vol. 17, no. 9, p. 78, 2021.
- [11] B. Ell, L. Mercatali, T. Ibrahim et al., "Tumor-induced osteoclast miRNA changes as regulators and biomarkers of osteolytic bone metastasis," *Cancer Cell*, vol. 24, no. 4, pp. 542–556, 2013.
- [12] S. Huang, K. Shao, Y. Liu et al., "Tumor-targeting and microenvironment-responsive smart nanoparticles for combination therapy of antiangiogenesis and apoptosis," *ACS Nano*, vol. 7, no. 3, pp. 2860–2871, 2013.
- [13] H. Li, Z. Qiu, F. Li, and C. Wang, "The relationship between MMP-2 and MMP-9 expression levels with breast cancer incidence and prognosis," *Oncology Letters*, vol. 14, no. 5, pp. 5865–5870, 2017.
- [14] K. Sakata, K. Shigemasa, N. Nagai, and K. Ohama, "Expression of matrix metalloproteinases (MMP-2, MMP-9, MT1-MMP) and their inhibitors (TIMP-1, TIMP-2) in common epithelial tumors of the ovary," *International Journal of Oncology*, vol. 17, no. 4, pp. 673–681, 2000.
- [15] E. E. Creemers, J. P. Cleutjens, J. F. Smits, and M. J. Daemen, "Matrix metalloproteinase inhibition after myocardial infarction: a new approach to prevent heart failure?" *Circulation Research*, vol. 89, no. 3, pp. 201–210, 2001.
- [16] C. M. Dollery, J. R. McEwan, and A. M. Henney, "Matrix metalloproteinases and cardiovascular disease," *Circulation Research*, vol. 77, no. 5, pp. 863–868, 1995.
- [17] L. Tjäderhane, H. Larjava, T. Sorsa, V. J. Uitto, M. Larmas, and T. Salo, "The activation and function of host matrix metalloproteinases in dentin matrix breakdown in caries lesions," *Journal of Dental Research*, vol. 77, no. 8, pp. 1622–1629, 1998.
- [18] D. Karayashveva, M. Glushkova, E. Boteva, V. Mitev, and T. Kadiyska, "Association study for the role of Matrix metalloproteinases 2 and 3 gene polymorphisms in dental caries susceptibility," *Archives of Oral Biology*, vol. 68, pp. 9–12, 2016.
- [19] L. R. L. Diniz, M. T. d S. Souza, J. N. Barboza, R. N. Almeida, and D. P. Sousa, "Antidepressant potential of cinnamic acids: mechanisms of action and perspectives in drug development," *Molecules*, vol. 24, no. 24, p. 4469, 2019.
- [20] A. Taherkhani, A. Orangi, S. Moradkhani, A. Jalalvand, and Z. Khamverdi, "Identification of potential anti-tooth-decay compounds from organic cinnamic acid derivatives by inhibiting matrix metalloproteinase-8: an in silico study," *Avicenna Journal of Dental Research*, vol. 14, no. 1, pp. 25–32, 2022.
- [21] A. Taherkhani, F. Ghonji, A. Mazaheri, M. P. Lohrasbi, Z. Mohamadi, and Z. Khamverdi, "Identification of potential glucosyltransferase inhibitors from cinnamic acid derivatives using molecular docking analysis: a bioinformatics study," *Avicenna Journal of Clinical Microbiology and Infection*, vol. 8, no. 4, pp. 145–155, 2021.
- [22] P. Su, Y. Shi, J. Wang, X. Shen, and J. Zhang, "Anticancer agents derived from natural cinnamic acids," *Anti-Cancer Agents in Medicinal Chemistry*, vol. 15, no. 8, pp. 980–987, 2015.
- [23] E. Pontiki and D. Hadjipavlou-Litina, "Antioxidant and anti-inflammatory activity of aryl-acetic and hydroxamic acids as novel lipoxygenase inhibitors," *Medicinal Chemistry*, vol. 2, no. 3, pp. 251–264, 2006.
- [24] E. Pontiki and D. Hadjipavlou-Litina, "Synthesis and pharmacological evaluation of novel aryl-acetic acid inhibitors of lipoxygenase, antioxidants, and anti-inflammatory agents," *Bioorganic & Medicinal Chemistry*, vol. 15, no. 17, pp. 5819–5827, 2007.
- [25] E. Pontiki, D. Hadjipavlou-Litina, G. Geromichalos, and A. Papageorgiou, "Anticancer activity and quantitative-structure activity relationship (QSAR) studies of a series of antioxidant/anti-inflammatory aryl-acetic and hydroxamic acids," *Chemical Biology & Drug Design*, vol. 74, no. 3, pp. 266–275, 2009.
- [26] W.-Y. Chung, Y.-J. Jung, Y.-J. Surh, S.-S. Lee, and K.-K. Park, "Antioxidative and antitumor promoting effects of [6]-paradol and its homologs," *Mutation Research: Genetic Toxicology and Environmental Mutagenesis*, vol. 496, no. 1–2, pp. 199–206, 2001.
- [27] D. P. Bezerra, F. O. Castro, A. P. Alves et al., "In vivo growth-inhibition of Sarcoma 180 by piplartine and piperine, two alkaloid amides from Piper," *Brazilian Journal of Medical and Biological Research*, vol. 39, no. 6, pp. 801–807, 2006.
- [28] S. Arranz, G. Chiva-Blanch, P. Valderas-Martinez, A. Medina-Remón, R. M. Lamuela-Raventós, and R. Estruch, "Wine, beer, alcohol and polyphenols on cardiovascular disease and cancer," *Nutrients*, vol. 4, no. 7, pp. 759–781, 2012.
- [29] S. Naz, S. Ahmad, S. Ajaz Rasool, S. Asad Sayeed, and R. Siddiqi, "Antibacterial activity directed isolation of compounds from *Onosma hispidum*," *Microbiological Research*, vol. 161, no. 1, pp. 43–48, 2006.
- [30] B. Shaker, S. Ahmad, J. Lee, C. Jung, and D. Na, "In silico methods and tools for drug discovery," *Computers in Biology and Medicine*, vol. 137, 2021.
- [31] A. L. Nazarova and V. Katritch, "It all clicks together: in silico drug discovery becoming mainstream," *Clinical and Translational Medicine*, vol. 12, no. 4, 2022.
- [32] O. H. Onyango, "In silico models for anti-COVID-19 drug discovery: a systematic review," *Advances in pharmacological and pharmaceutical sciences*, vol. 2023, pp. 1–15, 2023.
- [33] S. K. Burley, C. Bhikadiya, C. Bi et al., "RCSB Protein Data Bank: powerful new tools for exploring 3D structures of biological macromolecules for basic and applied research and education in fundamental biology, biomedicine, biotechnology, bioengineering and energy sciences," *Nucleic Acids Research*, vol. 49, no. D1, pp. D437–D451, 2021.
- [34] C. C. Chen and O. Herzberg, "Inhibition of β -lactamase by clavulanate: trapped intermediates in cryocrystallographic studies," *Journal of Molecular Biology*, vol. 224, no. 4, pp. 1103–1113, 1992.
- [35] E. Y. Lin, W. Xi, N. Aggarwal, and M. L. Shinohara, "Osteopontin (OPN)/SPP1: from its biochemistry to biological functions in the innate immune system and the central nervous system (CNS)," *International Immunology*, vol. 35, no. 4, pp. 171–180, 2023.
- [36] V. Dhanaraj, M. G. Williams, Q.-Z. Ye, F. Molina, L. L. Johnson, D. F. Ortwine et al., "X-ray structure of gelatinase A catalytic domain complexed with a hydroxamate inhibitor," *Croatica Chemica Acta*, vol. 72, no. 2–3, pp. 575–591, 1999.
- [37] D. S. Wishart, Y. D. Feunang, A. C. Guo et al., "DrugBank 5.0: a major update to the DrugBank database for 2018," *Nucleic Acids Research*, vol. 46, no. D1, pp. D1074–D1082, 2018.
- [38] Z. Bayat, A. Tarokhian, and A. Taherkhani, "Cinnamic acids as promising bioactive compounds for cancer therapy by targeting MAPK3: a computational simulation study," *Journal of*

- Complementary and Integrative Medicine*, vol. 20, no. 3, pp. 621–630, 2023.
- [39] M. H. Malekipour, F. Shirani, S. Moradi, and A. Taherkhani, “Cinnamic acid derivatives as potential matrix metalloproteinase-9 inhibitors: molecular docking and dynamics simulations,” *Genomics & Informatics*, vol. 21, no. 1, p. e9, 2023.
- [40] Y. Dinakarkumar, J. R. Rajabathar, S. Arokiyaraj et al., “Anti-methanogenic effect of phytochemicals on methyl-coenzyme M reductase—potential: in silico and molecular docking studies for environmental protection,” *Micromachines*, vol. 12, no. 11, p. 1425, 2021.
- [41] A. Taherkhani, A. Orangi, S. Moradkhani, and Z. Khamverdi, “Molecular docking analysis of flavonoid compounds with matrix metalloproteinase-8 for the identification of potential effective inhibitors,” *Letters in Drug Design and Discovery*, vol. 18, no. 1, pp. 16–45, 2021.
- [42] O. Trott and A. J. Olson, “AutoDock Vina: improving the speed and accuracy of docking with a new scoring function, efficient optimization, and multithreading,” *Journal of Computational Chemistry*, vol. 31, no. 2, pp. 455–461, 2010.
- [43] K. Zhu, K. W. Borrelli, J. R. Greenwood et al., “Docking covalent inhibitors: a parameter free approach to pose prediction and scoring,” *Journal of Chemical Information and Modeling*, vol. 54, no. 7, pp. 1932–1940, 2014.
- [44] R. A. Friesner, R. B. Murphy, M. P. Repasky et al., “Extra precision glide: docking and scoring incorporating a model of hydrophobic enclosure for protein–ligand complexes,” *Journal of Medicinal Chemistry*, vol. 49, no. 21, pp. 6177–6196, 2006.
- [45] Z. Azadian, S. Hosseini, Z. P. Dizjikan et al., “---dependent TGF- β pathways,” *Journal of Cellular Biochemistry*, vol. 123, no. 2, pp. 450–468, 2021.
- [46] M. Masumi, F. Noormohammadi, F. Kianisaba, F. Nouri, M. Taheri, and A. Taherkhani, “Methicillin-resistant *Staphylococcus aureus*: docking-based virtual screening and molecular dynamics simulations to identify potential penicillin-binding protein 2a inhibitors from natural flavonoids,” *International journal of microbiology*, vol. 2022, pp. 1–14, 2022.
- [47] A. Cetin, “Some flavolignans as potent SARS-CoV-2 inhibitors via molecular docking, molecular dynamic simulations and ADME Analysis,” *Current Computer-Aided Drug Design*, vol. 18, no. 5, pp. 337–346, 2022.
- [48] B. R. Brooks, C. L. Brooks, A. D. Mackerell et al., “CHARMM: the biomolecular simulation program,” *Journal of Computational Chemistry*, vol. 30, no. 10, pp. 1545–1614, 2009.
- [49] A. Daina, O. Michielin, and V. Zoete, “SwissADME: a free web tool to evaluate pharmacokinetics, drug-likeness and medicinal chemistry friendliness of small molecules,” *Scientific Reports*, vol. 7, no. 1, pp. 42717–42813, 2017.
- [50] P. Henriët and H. Emonard, “Matrix metalloproteinase-2: not (just) a hero of the past,” *Biochimie*, vol. 166, pp. 223–232, 2019.
- [51] E. Bueno-Gavilá, A. Abellán, F. Girón-Rodríguez et al., “Bioactivity of hydrolysates obtained from bovine casein using artichoke (*Cynara scolymus* L.) proteases,” *Journal of Dairy Science*, vol. 102, no. 12, pp. 10711–10723, 2019.
- [52] R. Upadhyay and L. J. Mohan Rao, “An outlook on chlorogenic acids-occurrence, chemistry, technology, and biological activities,” *Critical Reviews in Food Science and Nutrition*, vol. 53, no. 9, pp. 968–984, 2013.
- [53] S. Nunes, A. R. Madureira, D. Campos et al., “Therapeutic and nutraceutical potential of rosmarinic acid—cytoprotective properties and pharmacokinetic profile,” *Critical Reviews in Food Science and Nutrition*, vol. 57, no. 9, pp. 1799–1806, 2017.
- [54] D. B. Magalhães, I. Castro, V. Lopes-Rodrigues et al., “Melissa officinalis L. ethanolic extract inhibits the growth of a lung cancer cell line by interfering with the cell cycle and inducing apoptosis,” *Food & Function*, vol. 9, no. 6, pp. 3134–3142, 2018.
- [55] R. Hajiaghaee, H. R. Monsef-Esfahani, M. R. Khorramizadeh, F. Saadat, A. R. Shahverdi, and F. Attar, “Inhibitory effect of aerial parts of *Scrophularia striata* on matrix metalloproteinases expression,” *Phytotherapy Research*, vol. 21, no. 12, pp. 1127–1129, 2007.
- [56] H. R. Monsef-Esfahani, R. Hajiaghaee, A. R. Shahverdi, M. R. Khorramizadeh, and M. Amini, “Flavonoids, cinnamic acid and phenyl propanoid from aerial parts of *Scrophularia striata*,” *Pharmaceutical Biology*, vol. 48, no. 3, pp. 333–336, 2010.
- [57] G. C. Yen, Y. L. Chen, F. M. Sun, Y. L. Chiang, S. H. Lu, and C. J. Weng, “A comparative study on the effectiveness of cis- and trans-form of cinnamic acid treatments for inhibiting invasive activity of human lung adenocarcinoma cells,” *European Journal of Pharmaceutical Sciences*, vol. 44, no. 3, pp. 281–287, 2011.
- [58] C. Keskin, A. Ölçekçi, A. Baran et al., “Green synthesis of silver nanoparticles mediated *Diospyros kaki* L. (Persimmon): determination of chemical composition and evaluation of their antimicrobials and anticancer activities,” *Frontiers in Chemistry*, vol. 11, 2023.
- [59] J. Zhao, L. Xu, D. Jin et al., “Rosmarinic acid and related dietary supplements: potential applications in the prevention and treatment of cancer,” *Biomolecules*, vol. 12, no. 10, p. 1410, 2022.
- [60] Y. Xu, G. Xu, L. Liu, D. Xu, and J. Liu, “Anti-invasion effect of rosmarinic acid via the extracellular signal-regulated kinase and oxidation–reduction pathway in Ls174-T cells,” *Journal of Cellular Biochemistry*, vol. 111, no. 2, pp. 370–379, 2010.
- [61] Y.-H. Han, J.-Y. Kee, and S.-H. Hong, “Rosmarinic acid activates AMPK to inhibit metastasis of colorectal cancer,” *Frontiers in Pharmacology*, vol. 9, p. 68, 2018.
- [62] R. Masarwy, L. Kampel, G. Horowitz, O. Gutfeld, and N. Muhanna, “Neoadjuvant PD-1/PD-L1 inhibitors for resectable head and neck cancer: a systematic review and meta-analysis,” *JAMA Otolaryngology–Head & Neck Surgery*, vol. 147, no. 10, pp. 871–878, 2021.
- [63] L. Huang, J. Chen, J. Quan, and D. Xiang, “Rosmarinic acid inhibits proliferation and migration, promotes apoptosis and enhances cisplatin sensitivity of melanoma cells through inhibiting ADAM17/EGFR/AKT/GSK3 β axis,” *Bioengineered*, vol. 12, no. 1, pp. 3065–3076, 2021.
- [64] Z. Ma, J. Yang, Y. Yang et al., “Rosmarinic acid exerts an anticancer effect on osteosarcoma cells by inhibiting DJ-1 via regulation of the PTEN-PI3K-Akt signaling pathway,” *Phytomedicine*, vol. 68, 2020.
- [65] K. Yang, Z. Shen, Y. Zou, and K. Gao, “Rosmarinic acid inhibits migration, invasion, and p38/AP-1 signaling via miR-1225-5p in colorectal cancer cells,” *Journal of Receptors and Signal Transduction*, vol. 41, no. 3, pp. 284–293, 2021.
- [66] Y. Han, L. Ma, L. Zhao, W. Feng, and X. Zheng, “Rosmarinic inhibits cell proliferation, invasion and migration via up-regulating miR-506 and suppressing MMP2/16 expression in pancreatic cancer,” *Biomedicine & Pharmacotherapy*, vol. 115, 2019.
- [67] S. Mojtavavi, M. R. Khoshayand, M. R. Fazeli, M. A. Faramarzi, and N. Samadi, “Development of an

- enzyme-enhancer system to improve laccase biological activities,” *International Journal of Biological Macromolecules*, vol. 173, pp. 99–108, 2021.
- [68] S. Zhang, “Dental caries and vaccination strategy against the major cariogenic pathogen, *Streptococcus mutans*,” *Current Pharmaceutical Biotechnology*, vol. 14, no. 11, pp. 960–966, 2014.
- [69] G. F. Ferrazzano, I. Amato, A. Ingenito, A. De Natale, and A. Pollio, “Anti-cariogenic effects of polyphenols from plant stimulant beverages (cocoa, coffee, tea),” *Fitoterapia*, vol. 80, no. 5, pp. 255–262, 2009.
- [70] H. Koo, P. L. Rosalen, J. A. Cury et al., “Effect of a new variety of *Apis mellifera* propolis on mutans Streptococci,” *Current Microbiology*, vol. 41, no. 3, pp. 192–196, 2000.
- [71] S. Saleh, A. Salama, A. M. Ali, A. K. Saleh, B. A. Elhady, and E. Tolba, “Egyptian propolis extract for functionalization of cellulose nanofiber/poly (vinyl alcohol) porous hydrogel along with characterization and biological applications,” *Scientific Reports*, vol. 13, no. 1, p. 7739, 2023.